IEEE Access
Multidisciplinary : Rapid Review : Open Access Journal

Received 25 March 2026, accepted 5 April 2026, date of publication 8 April 2026, date of current version 17 April 2026.

Digital Object Identifier 10.1109/ACCESS.2026.3681898

RESEARCH ARTICLE

MCS-Based Small Signal Analysis of PMSG Wind Turbines: A Sensitivity Matrix Approach

YEONG GEON SON[1], **(Member, IEEE), AND SUNG-YUL KIM**[2], **(Member, IEEE)**
[1]Keimyung University, Daegu, South Korea
[2]Hanyang University, Seoul, South Korea

Corresponding author: Sung-Yul Kim (pslab2040@gmail.com)

This research was supported by Korea Electric Power Corporation (Grant number: R24XO03-2). This work was supported by the Korea Institute of Energy Technology Evaluation and Planning (KETEP) and the Ministry of Climate, Energy & Environment (MCEE) of the Republic of Korea (No. RS-2025-02313547).

ABSTRACT In this study, we propose a new approach to assess the stability of Permanent Magnet Synchronous Generator (PMSG) based wind turbines through a method of Small Signal Analysis (SSA) utilizing Monte Carlo Simulation (MCS). PMSG wind power systems are generally known to have high resistance to Sub-synchronous Oscillation (SSO), however, the potential for oscillations to occur is dependent on the serial compensation of transmission lines and the robustness of the connected grid. Therefore, stability analysis is necessary at the system connection planning stage of PMSG wind turbines. In this research, we presented a state-space model of PMSG wind turbines and derived a sensitivity matrix to analyze eigenvalues in response to parameter changes. Based on the sensitivity matrix, we grouped the main factors affecting the eigenvalues to facilitate MCS calculations. The results obtained from the MCS-based SSA method identify the stable and unstable regions of the PMSG wind turbines, providing selective solutions for the design of a stable PMSG wind power system.

INDEX TERMS Sensitivity matrix, PMSG wind turbine, Monte Carlo simulation, small signal analysis.

I. NOMENCLATURE

θ_1, θ_s	Blade and rotor angles.
ω_1, ω_s	Blade and rotor velocities.
M_1, M_2	Inertia moments of the blade and rotor.
D_1, D_2	Self-damping coefficients of the two masses.
D_{12}	Mutual damping coefficients between the two masses.
K_{12}	Stiffness shaft.
H_1, H_2	The inertia of the turbine and generator.
T_W, T_e	Aerodynamic torque and electromechanical torque from the generator.
V_{sd}, V_{sq}	d-axis and q-axis stator voltages.
i_{sd}, i_{sq}	d-axis and q-axis stator currents.
R_s	Stator resistance.
L_{sd}, L_{sq}	d and q-axis stator inductances.
ψ_f	Magnetic flux of the rotor.
ψ_{sd}, ψ_{sq}	d-axis and q-axis stator fluxes.
N_p	Number of poles.
K_i, K_p	Integration and proportionality coefficients.
L_c.	Filter inductance.
ω_e, ω_g	Electrical angular velocity of the rotor side converter and grid side converter.
V_{gd}, V_{gq}	d-axis and q-axis grid side converter voltages.
i_{gd}, i_{gq}	d-axis and q-axis grid side converter currents.
V_{DC}	DC-link voltage.
L_{line}	Transmission line inductance.
C_{line}	Transmission line capacitance.
R_{line}	Transmission line resistance.
i_{nd}, i_{nq}	d-axis and q-axis current on the transmission line.
V_{cd}, V_{cq}	Transmission line capacitance-voltage.

The associate editor coordinating the review of this manuscript and approving it for publication was Nga Nguyen.

II. INTRODUCTION

The continuous operation of coal-fired generators leads to carbon emissions, causing environmental pollution and global warming. In response, there is a global trend towards increasing the proportion of renewable energy sources to mitigate global warming through policies such as carbon neutrality. [1].

Wind turbines are classified into four types as one of the major sources of renewable energy generation. Type 1, the fixed-speed wind turbine, operates at a single speed without mechanical or electrical adjustments, maintaining a constant speed. However, it has the disadvantage of being inefficient due to its inability to flexibly respond to varying wind conditions [2]. Type 2, the variable-slip wind turbine, adjusts the slip rate to respond to wind speeds, allowing partial control over the turbine's rotational speed, but it has the limitation of a restricted adjustment range [3]. Type 3, the doubly-fed induction generator wind turbine, can operate at variable speeds by receiving power from both the rotor and the stator, offering a flexible response to wind variations. However, it is more maintenance-intensive and has lower energy conversion efficiency compared to Type 4 [4]. Type 4, the permanent magnet synchronous generator (PMSG) wind turbine, operates independently from the power grid across the entire output voltage range through a converter, fully accommodating fluctuating wind conditions. It shows superior performance in efficiency, maintenance, and control aspects compared to Types 1-3, making it increasingly popular [5], [6]. Therefore, this study focuses on PMSG wind turbines.

The electricity generated through wind turbines serves as a clean energy source, offering environmentally friendly benefits, thus positively impacting the environment as its share increases. However, vibrations caused by resonance phenomena can lead to mechanical and electrical damage, presenting a drawback. Sub-synchronous oscillation (SSO) is a phenomenon found within power systems, referring to vibrations that occur at frequencies lower than the utility frequency in specific parts of the generator or power network [7]. SSO is mainly classified into three types based on its causes and characteristics. Sub-synchronous control interaction (SSCI) primarily occurs due to interactions between power electronic-based control systems and the power system [8]. Sub-synchronous torsional interaction (SSTI) stems from interactions between torsional vibrations existing between the turbine and generator and the power system [9]. Sub-synchronous resonance (SSR) is a resonance phenomenon that occurs due to interactions between the generator and the power network within the power system. It is particularly evident when the electrical resonance and mechanical resonance of a generator combine in transmission lines equipped with series capacitors [10].

This phenomenon was first identified in 1971 at the Mohave Power Station, and subsequent occurrences have been continuously reported since then [11]. SSO arises from the interactions among generators, controllers, and transmission lines, which can result in anything from damage to the generators to failures in the power system, thus necessitating its elimination. Reference [12] categorizes the incidence of SSO according to the type of wind turbine, noting that while Types 1-3 wind turbines are at a higher risk of resonance, Type 4 wind turbines have a higher immunity to torsional oscillation compared to other types, although they are still susceptible to vibrations caused by L-C circuits. Reference [13] also analyzes the potential for SSO occurrence by wind turbine type, mentioning that Type 4 wind turbines are relatively immune to SSO. Moreover, the occurrence of SSO across different wind turbine types has been extensively investigated in various studies [14], [15].

According to the literature, PMSG wind turbines are generally known to have high immunity to SSO. However, vibrations can be induced by line compensation devices such as series capacitors installed in the connected transmission lines, and the possibility of SSO occurrence increases if the robustness of the connected system is weak [16]. For these reasons, research on the SSO issue in PMSG wind turbines is essential. Various methods to mitigate SSO have been proposed, and numerous studies have presented a range of solutions.

Reference [17] deals with the vibration issues that can arise when PMSG wind turbines are connected to weak AC grids. This study proposes a method to effectively mitigate vibrations using grid-forming control technology. Reference [18] suggests improving grid stiffness by applying a Battery Energy Storage System (BESS)-linked Synchronous Compensator (STATCOM) to address the SSO problem.

Not only is it important to effectively mitigate SSO, but preemptively detecting its occurrence is also crucial. Early detection of SSO allows for the swift implementation of appropriate protective measures, preventing potential damage and maintaining the overall stability of the system. Therefore, the development of SSO detection and mitigation technologies is essential for the stable operation and integration of PMSG wind turbines and other generation systems, necessitating continuous research and development.

Among the prominent methods used for detecting SSO are frequency analysis and small signal analysis (SSA). Frequency analysis involves converting time-domain data of voltage, current, and active power obtained through Electromagnetic Transients (EMT) models into the frequency domain to identify resonance frequency bands. The most used technique in this process is the Fast Fourier Transform (FFT). FFT allows for the conversion of time-domain data into the frequency domain for analysis, effectively identifying resonance phenomena such as SSO [19]. Reference [20] suggests that FFT and wavelet transform can be used for SSO detection. Reference [21] mentions that SSO can occur in PMSG wind turbines due to connections with systems of low robustness, applying FFT for SSO detection to identify sub-synchronous and super-synchronous oscillations at 14Hz and 86Hz, respectively. While frequency analysis is useful for identifying the frequency components of a signal, it does not directly analyze the dynamic stability or response characteristics of a system, focusing more on signal analysis than on design optimization. In contrast, SSA is essential for evaluating and optimizing the performance of feedback loops in control systems or power system designs. This allows designers to improve the system's response and meet desired performance metrics [22].

Reference [23] analyzes stability based on the eigenvalue loci within the complex coordinate system through SSA, based on dynamic modeling of PMSG wind turbines. Reference [23] validates SSA by comparing state space-based SSA, derived from dynamic modeling of PMSG wind turbine, with PSCAD/EMTDC models. References [24] and [25] utilize both frequency analysis and SSA simultaneously to detect SSO that may occur when connecting PMSG wind turbines with systems of low robustness, validating the methodology through the results. References [26] and [27] detail the dynamic modeling of PMSG wind turbines to construct the necessary state space for SSA analysis. Reference [28] mentions the possibility of SSO occurrence in PMSG wind turbines due to series compensated transmission, conducting both frequency analysis and SSA for SSO detection. Consequently, sub-synchronous and super-synchronous oscillations are detected at 17Hz and 83Hz, respectively.

In this study, we propose a SSA technique based on Monte Carlo Simulation (MCS) to assess the stability of PMSG wind turbines. MCS is a computer-based numerical technique that uses probabilistic or random processes to solve physical, economic, and mathematical problems, with detailed information available in Reference [29].

The proposed algorithm distinguishes itself significantly from existing methods of SSO analysis. It identifies and categorizes the parameters of PMSG wind turbines that influence the eigenvalues derived from SSA through a sensitivity matrix. Each group becomes a target for MCS, and the outcome of the simulation provides combinations of parameters that lead to system instability when PMSG wind turbines are connected, as well as combinations that result in a stable system. This offers grid operators and wind turbine operators a wide range of options for ensuring system stability, thereby providing economic benefits and high-quality grid stability. In contrast to existing literature that analyzes the phenomenon of SSO in PMSG wind turbines, this paper proposes an algorithm to avoid SSO. Our focus is on detecting SSO in PMSG wind turbines due to grid connection, hence concentrating on vibrations caused by L-C.

The primary contributions of the algorithm proposed in this paper are as follows:

1) The proposed algorithm is based on data interpretation, making it easily applicable to any system that can be analyzed for stability using State Space. This ensures excellent accessibility and compatibility of the algorithm.
2) When the information about the serial resistance and inductance connected to the PMSG wind turbine is determined, it becomes possible to select a range of available capacitances. This allows for effective reactive power compensation in lines connected to PMSG wind turbines.
3) The algorithm can be used not only to derive stable line information from the perspective of system operators but also to secure stable PMSG wind turbine design parameters from the perspective of PMSG wind turbine designers, demonstrating the excellent scalability of the algorithm.

The proposed algorithm has a clear logic involving: i) Differential equations and State Space modeling of PMSG wind turbine, ii) Sensitivity matrix modeling, iii) Grouping for MCS, iv) Applying MCS-based SSA to identify stable and unstable system regions, v) Model validation using SIMULINK/EMTDC models.

III. SYSTEM MODELING

A. BASIC STATE SPACE MODELING

The state space model is one of the methods for mathematically representing dynamic systems, describing the state of the system and how this state changes over time. This model can be applied to both linear and nonlinear systems and clearly expresses the relationships among the system's inputs, outputs, and states in the time domain [30]. Eq. (1) represents the general form of the state space, as referenced in [31].

$$\begin{aligned} \frac{d}{dt}\Delta \boldsymbol{X}_k &= \boldsymbol{A}_k\Delta \boldsymbol{X}_k + \boldsymbol{B}_k\Delta \boldsymbol{V}_k \\ \Delta \boldsymbol{Y}_k &= \boldsymbol{C}_k\Delta \boldsymbol{X}_k, \quad k = 1, 2 \ldots, M \end{aligned} \tag{1}$$

where Δ refers to a small increment of a variable or variable vector, $\boldsymbol{X}_k$ is the vector of all the state variables of the kth PMSG wind turbine, $\Delta \boldsymbol{Y}_k = [\Delta Y_{kx} \Delta Y_{ky}]^T$ and $\Delta \boldsymbol{V}_k = [\Delta V_{kx} \Delta V_{ky}]^T$. In the absence of considering the direct transmission matrix, $\boldsymbol{A}_k, \boldsymbol{B}_k$ *and* $\boldsymbol{C}_k$ respectively represent the state transition matrix, input matrix, and output matrix. We focus on analyzing the dynamic state of the system to model the state space, and the full-order linearized model is as Eq. (2).

$$\frac{d}{dt}\Delta \boldsymbol{X} = \boldsymbol{A}\Delta \boldsymbol{X} \tag{2}$$

where $\Delta \boldsymbol{X} = [\Delta \boldsymbol{X}_1^T \Delta \boldsymbol{X}_2^T \cdots \Delta \boldsymbol{X}_M^T]^{\boldsymbol{T}}$, $\boldsymbol{A} = diag\,[\boldsymbol{A}_k] + diag\,[\boldsymbol{B}_k]\,\boldsymbol{X}_E\; diag\,[\boldsymbol{C}_k]$, $diag\,[\boldsymbol{A}_k], diag\,[\boldsymbol{B}_k], diag[\boldsymbol{C}_k]$ are diagonal block matrices with the diagonal element matrices to be $\boldsymbol{A}_k,\ \boldsymbol{B}_k$ *and* $\boldsymbol{C}_k,\ k = 1, 2, \ldots, M$, respectively.

In this paper, the state space model of the PMSG wind turbine is categorized into the drive train, synchronous generator, rotor-side converter (RSC), DC-link, grid-side converter (GSC), transmission line, and phase-locked loop (PLL) module. Each of these modules is reconstituted into the state space through a linear model as shown in Eq. (2).

B. BASIC STATE SPACE MODELING

In this study, the target PMSG wind turbine is a single wind turbine with a capacity of 8MW, utilizing a model connected through the drive train module, converter, and transmission line. Fig. 1 shows a simplified diagram of the PMSG wind turbine.

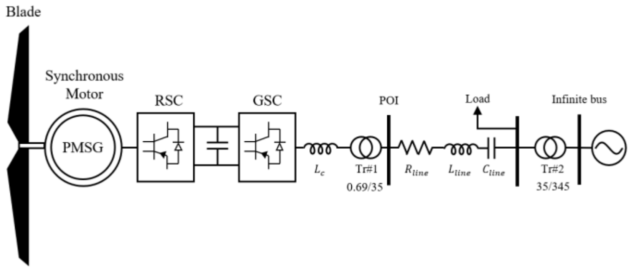

FIGURE 1. Diagram of PMSG wind turbine.

The drive train module is the transmission element that constitutes mechanical energy from the turbine blades, which rotate under the force of the wind, to the generator. Since the PMSG wind turbine does not have a gearbox, the blade rotor is applied as a two-mass model. The dynamic equation of the drive train module is shown in Eq. (3).

$$\Delta\dot{\theta}_1 = \Delta\omega_1 \tag{3a}$$
$$\Delta\dot{\theta}_2 = \Delta\omega_2 \tag{3b}$$
$$M_1\Delta\dot{\omega}_1 = \Delta T_W - D_1\omega_1 - D_{12}(\omega_1 - \omega_2) - K_{12}(\theta_1 - \theta_2) \tag{3c}$$
$$M_2\Delta\dot{\omega}_2 = -\Delta T_e - D_2\omega_2 - D_{12}(\omega_2 - \omega_1) - K_{12}(\theta_2 - \theta_1) \tag{3d}$$

The state space model of the drive train module is defined by state variables $\Delta \boldsymbol{X_D} = [\Delta\theta_1 \Delta\theta_2 \Delta\omega_1 \Delta\omega_2]^T$, input variables $\Delta \boldsymbol{V_D} = [\Delta T_W \Delta T_e]^T$ and output variables $\Delta \boldsymbol{Y_D} = [\Delta\theta_2 \Delta\omega_2]^T$.

The synchronous generator model applies the dynamics equations of the PMSG wind turbine, and the dynamics equations for stator voltages and stator currents, which have d-q axes, are as shown in Eq. (4).

$$V_{sd} = R_s i_{sd} + L_{sd}\frac{di_{sd}}{dt} - \omega_s L_{sq} i_{sq} \tag{4a}$$
$$V_{sq} = R_s i_{sq} + L_{sq}\frac{di_{sq}}{dt} - \omega_s L_{sd} i_{sd} + \omega_s \psi_f \tag{4b}$$

In Eq. (4), it is assumed that L_{sd} and L_{sq} are equal. The electromagnetic torque of the PMSG wind turbine is shown in Eq. (5).

$$T_e = -\frac{3}{2}N_p[(L_{sd} - L_{sq})i_{sd}i_{sq} + \psi_f i_{sq}] \tag{5}$$

The state space model of the synchronous generator module is characterized by state variables, $\Delta \boldsymbol{X_G} = \left[\Delta i_{sd} \Delta i_{sq}\right]^T$, input variables $\Delta \boldsymbol{V_G} = \left[\Delta V_{sd} \Delta V_{sq}\right]^T$ and output variables $\Delta \boldsymbol{Y_G} = \left[\Delta i_{sd} \Delta i_{sq} \Delta T_e\right]^T$. Fig. 2 provides a simplified illustration of the Two-mass model of the drive train to aid in understanding.

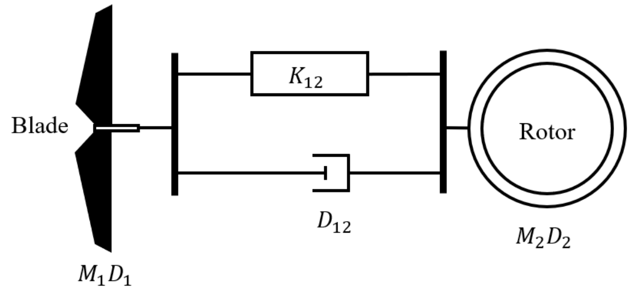

FIGURE 2. Two-mass model of drive train model.

The converter of the PMSG wind turbine is categorized into rotor-side and grid-side, and the two converters are connected through the DC link.

Fig. 3 shows the control logic of the RSC.

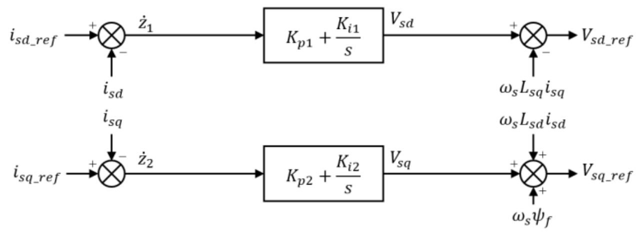

FIGURE 3. Diagram of RSC control logic.

According to the control logic shown in Fig. 3, the dynamic equation of the RSC is as shown in Eq. (6).

$$i_{sd\_ref} = 0 \tag{6a}$$
$$i_{sq\_ref} = -\frac{2T_{e\_ref}}{3N_p\psi_f} \tag{6b}$$
$$\dot{z}_1 = i_{sd\_ref} - i_{sd} \tag{6c}$$
$$\dot{z}_2 = i_{sq\_ref} - i_{sq} \tag{6d}$$
$$V_{sd\_ref} = \dot{z}_1 K_{p1} + z_1 K_{i1} - \omega_s L_{sq} i_{sq} \tag{6e}$$
$$V_{sq\_ref} = \dot{z}_2 K_{p2} + z_2 K_{i2} + \omega_s L_{sd} i_{sd} + \omega_s \psi_f \tag{6f}$$

The state space model of the RSC module is defined by state variables $\Delta \boldsymbol{X_{RSC}} = [\Delta x_1 \Delta x_2]^T$, input variables $\Delta \boldsymbol{V_{RSC}} = \left[\Delta i_{sd} \Delta i_{sq} \Delta\omega_s\right]^T$ and output variables $\Delta \boldsymbol{Y_{RSC}} = \left[\Delta V_{sd} \Delta V_{sq}\right]^T$.

Fig. 4 shows the control logic of the GSC.

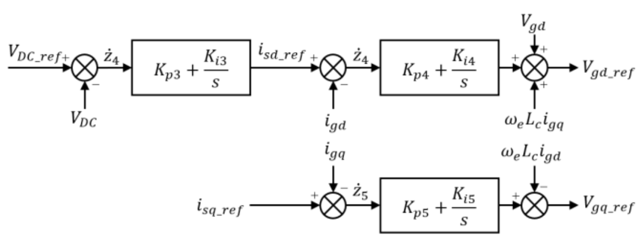

FIGURE 4. Diagram of GSC control logic.

According to the control logic shown in Fig. 4, the dynamic equation of the GSC is as shown in Eq. (7).

$$\dot{z}_3 = V_{DC\_ref} - V_{DC} \tag{7a}$$
$$\dot{z}_4 = i_{gd\_ref} - i_{gd} \tag{7b}$$
$$\dot{z}_5 = i_{gq\_ref} - i_{gq} \tag{7c}$$
$$i_{gd\_ref} = \dot{z}_3 K_{p3} + z_3 K_{i3} \tag{7d}$$
$$V_{gd\_ref} = \dot{z}_4 K_{p4} + z_4 K_{i4} + V_{gd} + \omega_e L_c i_{gq} \tag{7e}$$
$$V_{gq\_ref} = \dot{z}_5 K_{p5} + z_5 K_{i5} - \omega_e L_c i_{gd} \tag{7f}$$

The state space model of the GSC module is defined by state variables $\Delta \boldsymbol{X_{GSC}} = [\Delta x_3 \Delta x_4 \Delta x_5]^T$, input variables $\Delta \boldsymbol{V_{GSC}} = \left[\Delta i_{gd} \Delta i_{gq} \Delta \omega_e\right]^T$ and output variables $\Delta \boldsymbol{Y_{GSC}} = \left[\Delta V_{gd} \Delta V_{gq}\right]^T$.

The Dynamic equation connecting the RSC and GSC through the DC-link is shown in Eq. (8).

$$CV_{DC} \Delta \dot{V}_{DC} = V_{gd} i_{gd} + V_{gq} i_{gq} - V_{sd} i_{sd} - V_{sq} i_{sq} \tag{8}$$

The state space model of the DC-link module is defined by state variables $\Delta \boldsymbol{X_{DC}} = [\Delta V_{DC}]$, input variables $\Delta \boldsymbol{V_{DC}} = \left[\Delta V_{gq} \Delta V_{gd} \Delta i_{gq} \Delta i_{gd} \Delta V_{sq} \Delta V_{sd} \Delta i_{sq} \Delta i_{sd}\right]^T$ and output variables $\Delta \boldsymbol{Y_{DC}} = [\Delta V_{DC}]$.

The transmission line connects the PMSG wind turbine to the grid and is composed of RLC components in series. The dynamic equation of the transmission line is shown in Eq. (9).

$$L_{line} \frac{di_{nd}}{dt} = -R_{line} i_{nd} + \omega_g L_{line} i_{nq} - V_{cd} + V_{nd} - V_{gq} \tag{9a}$$
$$L_{line} \frac{di_{nq}}{dt} = -R_{line} i_{nq} + \omega_g L_{line} i_{nd} - V_{cq} + V_{nq} - V_{gq} \tag{9b}$$
$$C_{line} \frac{dV_{cd}}{dt} = i_{nd} + \omega_g C_{line} V_{cq} \tag{9c}$$
$$C_{line} \frac{dV_{cq}}{dt} = i_{nq} - \omega_g C_{line} V_{cd} \tag{9d}$$

The state space model of the transmission line module is defined by state variables $\Delta \boldsymbol{X_{RLC}} = \left[\Delta i_{nd} \Delta i_{nq} \Delta V_{cd} \Delta V_{cq}\right]^T$, input variables $\Delta \boldsymbol{V_{RLC}} = \left[\Delta V_{nd} \Delta V_{nq} \Delta V_{cd} \Delta V_{cq} \omega_g\right]^T$ and output variables $\Delta \boldsymbol{Y_{RLC}} = \left[\Delta i_{nd} \Delta i_{nq}\right]^T$.

The PLL functions to track the phase of the input signal and synchronize the phase of its oscillating signal with that of the input signal. The dynamic equation of the PLL is shown in Eq. (10).

$$\frac{dx_a}{dt} = V_{gq} \tag{10a}$$
$$\frac{dx_b}{dt} = \omega_0 + k_{ppll} V_{gq} + V_{gq} \frac{k_{ipll}}{s} \tag{10b}$$

The state space model of the PLL module is defined by state variables $\Delta \boldsymbol{X_{PLL}} = [\Delta x_a \Delta x_b]^T$, input variables $\Delta \boldsymbol{V_{PLL}} = \left[\Delta V_{gq}\right]^T$ and output variables $\Delta \boldsymbol{Y_{PLL}} = \left[\Delta \omega_g\right]^T$.

The total state variables established from the previously modeled dynamic equations on the PMSG wind turbine are shown in Eq. (11).

$$\boldsymbol{X} = \begin{bmatrix} \Delta\theta_1\ \Delta\theta_2\ \Delta\omega_1\ \Delta\omega_2\ \Delta i_{sd}\ \Delta i_{sq}\ \Delta V_{DC}\ \Delta z_1\ \Delta z_2 \\ \Delta z_3\ \Delta z_4\ \Delta z_5\ \Delta i_{nd}\ \Delta i_{nq}\ \Delta u_{cd}\ \Delta u_{cq}\ \Delta x_a\ \Delta x_b \end{bmatrix} \tag{11}$$

Those 18 state variables are numbered with $\boldsymbol{X}_k (k = 1, 2, \ldots, 18)$.

IV. PROPOSED ALGORITHM

A. SENSITIVITY MATRIX

In this paper, the proposed algorithm is based on Monte Carlo Simulation (MCS)-based Small Signal Analysis (SSA), necessitating the selection of parameters for MCS application. The calculated state space of the PMSG wind turbine in this paper, with $\boldsymbol{X} \in \mathbb{R}^{\mathbf{18}}$ and $\boldsymbol{A} \in \mathbb{R}^{\mathbf{18\times18}}$, indicates that up to 18 eigenvalues can influence the system's stability. These eigenvalues are calculated through det($\boldsymbol{A} - \lambda \boldsymbol{I}$). The system parameters affecting these 18 eigenvalues satisfy $\boldsymbol{\gamma}_m \in \boldsymbol{A}^{k\times k}$ $(k = 1, 2, \ldots, 18)$, where m represents the number of system parameters. The method of determining stability through SSA in control systems is based on the location of the real parts of the eigenvalues; if the real part of an eigenvalue settles in the Left Half Plane (LHP), the system is stable. If it settles in the Right Half Plane (RHP), the system is unstable. If it is 0, the system is considered marginally stable. Therefore, this paper limits the determination of system stability to the real parts of the eigenvalues.

Applying all parameters m simultaneously as targets for MCS in complex state space models leads to excessive computational time and makes it difficult to discern all possible solutions. Therefore, we categorize and group $\boldsymbol{\gamma}_m$, the parameters influencing the real parts of the eigenvalues derived through matrix $\boldsymbol{A}$. The sensitivity matrix is formed based on the derivatives of the real parts of the eigenvalues for each parameter change in $\boldsymbol{\gamma}_m$. The sensitivity matrix $\boldsymbol{M} \in \mathbb{R}^{\boldsymbol{m\times k}}$ is shown in Eq. (12).

The sensitivity matrix serves as a quantitative measure of how each parameter influences the real parts of the eigenvalues, enabling the identification of dominant parameter–mode interactions. By analyzing the magnitude and distribution of the sensitivity values, parameters with negligible impact can be excluded from the MCS process, while the most influential parameters are selectively retained.

This screening process effectively reduces the dimensionality of the parameter space and mitigates the computational burden associated with full-scale MCS, particularly in high-dimensional systems. As a result, the proposed approach allows efficient exploration of stability boundaries without compromising the accuracy of instability detection.

$$\boldsymbol{M}_{km} = \frac{d\boldsymbol{\lambda}_k}{d\boldsymbol{\gamma}_m} = \begin{bmatrix} \frac{d\lambda_1}{d\gamma_1} & \cdots & \frac{d\lambda_k}{d\gamma_1} \\ \vdots & \ddots & \vdots \\ \frac{d\lambda_1}{d\gamma_m} & \cdots & \frac{d\lambda_k}{d\gamma_m} \end{bmatrix}, \quad \forall k, \forall m \tag{12}$$

The sensitivity matrix represents the trend of change in the real parts of eigenvalues as each parameter increases.

TABLE 1. Sensitivity matrix of PMSG wind turbine.

MCS Group		γ_m	Number of eigenvalues k																	
			1	2	3	4	5	6	7	8	9	10	11	12	13	14	15	16	17	18
i)	1	K_{i1}	0	-1	0	0	0	0	0	0	0	0	0	0	0	0	0	0	0	0
	2	K_{i2}	0	0	-1	0	0	0	0	0	0	0	0	0	0	0	0	0	0	0
	3	K_{i3}	0	0	0	-1	0	0	0	0	0	0	0	0	0	0	0	0	0	0
	4	K_{i4}	0	0	0	-1	-1	0	0	0	0	0	0	0	0	0	0	0	0	0
	5	K_{i5}	0	0	0	0	0	-1	0	0	0	0	0	0	0	0	0	0	0	0
	6	K_{ipll}	0	0	0	0	0	0	0	0	0	0	0	0	0	0	0	0	0	0
	7	K_{p1}	0	+1	0	0	0	0	0	0	0	0	0	0	0	0	0	0	0	0
	8	K_{p2}	0	0	+1	0	0	0	0	0	0	0	0	0	0	0	0	0	0	0
	9	K_{p3}	0	0	0	+1	0	0	0	0	0	0	0	0	0	0	0	0	0	0
	10	K_{p4}	0	0	0	+1	+1	0	0	0	0	0	0	0	0	0	0	0	0	0
		K_{p5}	0	0	0	0	0	+1	0	0	0	0	0	0	0	0	0	0	0	0
	11	K_{ppll}	0	0	0	0	0	0	0	0	0	0	0	0	0	0	0	0	0	0
ii)	12	L_{line}	0	0	0	0	0	0	0	0	0	0	0	0	0	0	+1	+1	-1	-1
	13	C_{line}	0	0	0	0	0	0	0	0	0	0	0	0	0	0	+1	+1	-1	-1
	14	R_{line}	0	0	0	0	0	0	0	0	0	0	0	0	0	0	-1	-1	+1	+1
iii)	15	D_1	0	0	0	0	0	0	0	0	0	0	+1	+1	+1	-1	0	0	0	0
	16	D_2	0	0	0	0	0	0	0	0	0	0	-1	-1	0	-1	0	0	0	0
	17	D_{12}	0	0	0	0	0	0	0	0	-1	-1	-1	-1	1	1	0	0	0	0
	18	M_1	0	0	0	0	0	0	0	0	+1	+1	+1	+1	0	1	0	0	0	0
	19	M_2	0	0	0	0	0	0	0	0	+1	+1	+1	+1	-1	0	0	0	0	0
	20	k_{12}	0	0	0	0	0	0	0	0	-1	-1	+1	-1	0	0	0	0	0	0
	21	R_s	0	0	0	0	0	0	0	0	-1	-1	-1	-1	0	0	0	0	0	0
	22	L_{sd}	0	0	0	0	0	0	0	0	+1	+1	-1	+1	-1	-1	0	0	0	0
	23	L_{sq}	0	0	0	0	0	0	0	0	+1	+1	-1	+1	-1	-1	0	0	0	0

As described in Eq. (12), if there is no change with the parameter increase, it is marked as 0. If the change in the real parts of eigenvalues is directly proportional to the parameter change, it is denoted as +1, and if it is inversely proportional, it is denoted as -1.

$$\boldsymbol{M}_{km} = \begin{cases} 0, & \text{if } \dfrac{d\boldsymbol{\lambda}_k}{d\boldsymbol{\gamma}_m} = 0 \\ +1, & \text{if } \dfrac{d\boldsymbol{\lambda}_k}{d\boldsymbol{\gamma}_m} > 0 \\ -1, & \text{if } \dfrac{d\boldsymbol{\lambda}_k}{d\boldsymbol{\gamma}_m} < 0 \end{cases}, \quad \forall k, \forall m \tag{13}$$

Through Eq. (13), $\boldsymbol{\gamma}_m$ affecting $\boldsymbol{\lambda}_k$ can be detected. Table. 1 presents the sensitivity matrix derived for the state space of the PMSG wind turbine discussed in this paper.

For the derivation of the sensitivity matrix, the variation of $\boldsymbol{\gamma}_m$ is chosen from 50% to 150% relative to the reference value, and a 100-partition simulation is applied for each $\boldsymbol{\gamma}_m$. The parameter variation range from 50% to 150% of the nominal value was selected as a symmetric perturbation interval to capture both increasing and decreasing trends in eigenvalue sensitivity

Through the sensitivity matrix, it is identified that eigenvalues 2 to 6 are influenced by control system parameters, eigenvalues 9 to 14 are influenced by generator design parameters, and eigenvalues 15 to 18 are influenced by transmission line parameters. Therefore, MCS is categorized into three separate groups: *i) the MCS group for the control section of the PMSG wind turbine, ii) the MCS group for the connected transmission line, and iii) the MCS group for the design of the PMSG wind turbine*. Each MCS groups do not influence eigenvalues outside of their group, and among the eigenvalues, there are factors such as the 7th and 8th eigenvalues that are not affected by any parameter changes designed in this paper.

The transmission-line parameters (R, L, and C) also reflect the effective grid strength seen from the point of interconnection. In general, a weaker grid corresponds to a higher equivalent impedance, which can reduce damping and increase the risk of oscillatory instability.

In this paper, we focus on detecting SSO according to the RLC combination of the transmission line for system connection, thus only considering ii) the MCS group for the connected transmission line.

The sensitivity matrix also provides practical guidance for controller tuning by indicating the direction in which each parameter should be adjusted to improve system damping.

B. SSA BASED ON MCS

For an efficient SSA based on MCS, the parameters affecting the eigenvalues are grouped based on the results of the preceding Sensitivity matrix, following Eqs. (14)-(16).

$$[K_{il}, K_{pl}] \in G_{MCS\_i}, l = 1, 2 \ldots, 5 \tag{14}$$

$$[L_{line}, C_{line}, R_{line}] \in G_{MCS\_ii} \tag{15}$$

$$[D_1, D_2, D_{12}, M_1, M_2, k_{12}, R_s, L_s] \in G_{MCS\_iii} \tag{16}$$

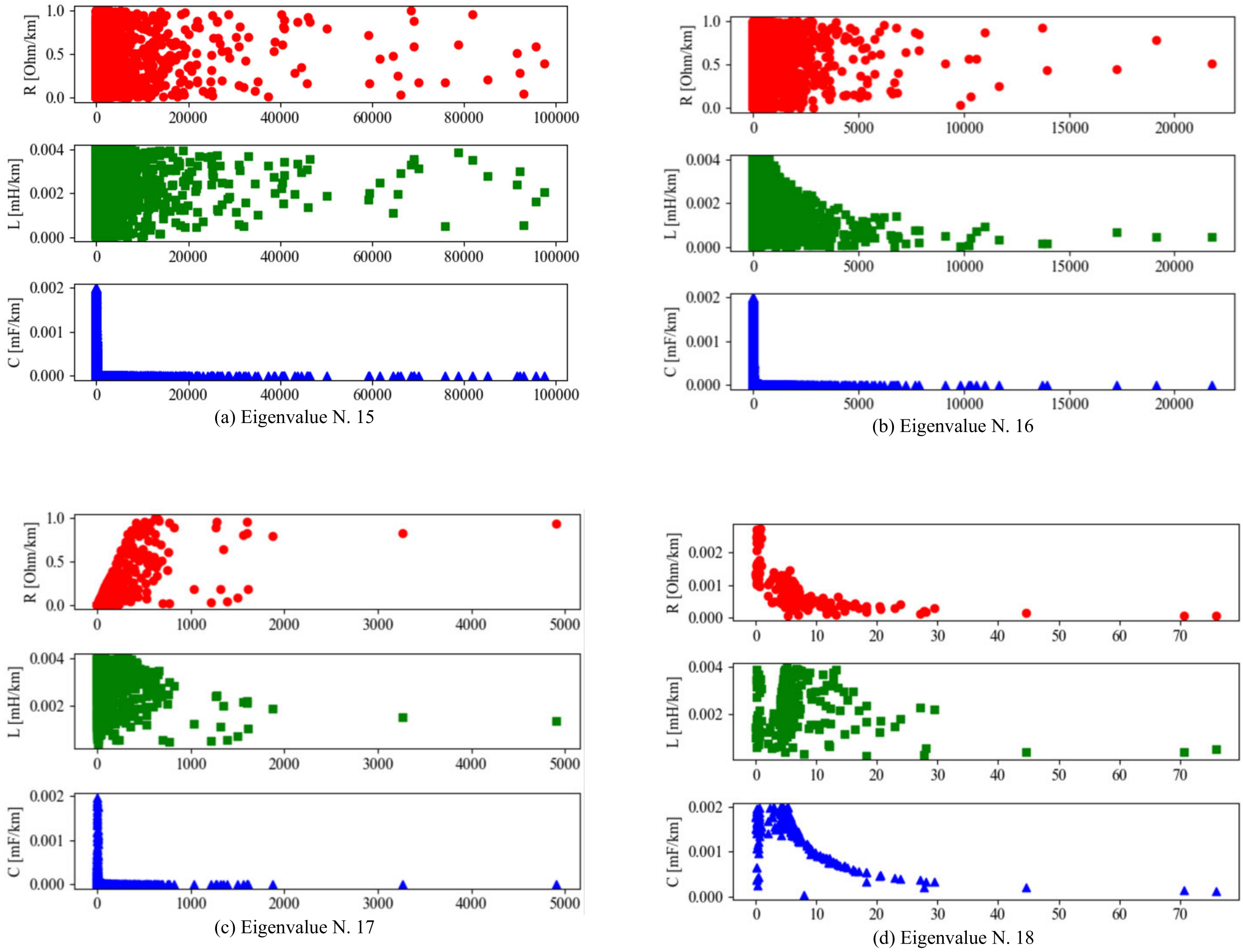

FIGURE 5. Eigenvalues on the RHP.

As mentioned earlier in this paper we focus on the SSO due to the components of the transmission line, therefore only G_{MCS_iii} is considered.

Sequentially examining all combinations of parameters within the same MCS group can be quite challenging. Therefore, in this paper, we randomly set the parameters within the same MCS group and derive the system's stable and unstable regions and the combinations of parameters through countless simulations. Consequently, the matrix **A** for deriving eigenvalues is applied as shown in Eqs. (17) and (18).

$$\boldsymbol{A} = [\boldsymbol{A}_D \boldsymbol{A}_G \boldsymbol{A}_{RSC}\ \boldsymbol{A}_{DC} \boldsymbol{A}_{GSC} \boldsymbol{A}_{RLC}(\tau) \boldsymbol{A}_{PLL}\ ] \quad (17)$$

$$\boldsymbol{A}_{RLC}(\tau) = f\ (\boldsymbol{R}(\tau),\ \boldsymbol{L}(\tau),\ \boldsymbol{C}(\tau)) \quad (18)$$

$$\overline{R} \leq \boldsymbol{R}(\tau) \leq \underline{R} \quad (19)$$

$$\overline{L} \leq \boldsymbol{L}(\tau) \leq \underline{L} \quad (20)$$

$$\overline{C} \leq \boldsymbol{C}(\tau) \leq \underline{C} \quad (21)$$

The (τ) represents a random function. Eq. (18) implies that $\boldsymbol{A}_{RLC}$ is determined by the random functions of R, L, and C. Eqs (19)-(21) refer to the bound of each random variable.

A total of 1,000,000 Monte Carlo samples were used to ensure sufficient coverage of the parameter space and reliable identification of the stability boundary.

In large-scale wind farm systems, the application of full-scale MCS is computationally challenging due to the high dimensionality of the parameter space, strong parameter coupling, and the increased computational cost of repeated eigenvalue analysis.

V. SIMULATION RESULTS

Having selected the target group through the sensitivity matrix, the elements subject to MCS application are limited to R, L, and C. To detect SSO in PMSG wind turbines, we expand the ranges of R, L, and C using a random function. The range for R is chosen to be 0.04 $\sim$ 1Ω/km, for L is 0.2 $\sim$ 0.004 mH/km, and for C is 0.01 $\sim$0.002 mF/km. The MCS is applied with 1,000,000 iterations. The simulation computer's CPU is a 12th Gen Intel(R) Core(TM) i9-12900KF (24 CPUs), $\sim$3.2GHz, and the total simulation time was 934 seconds.

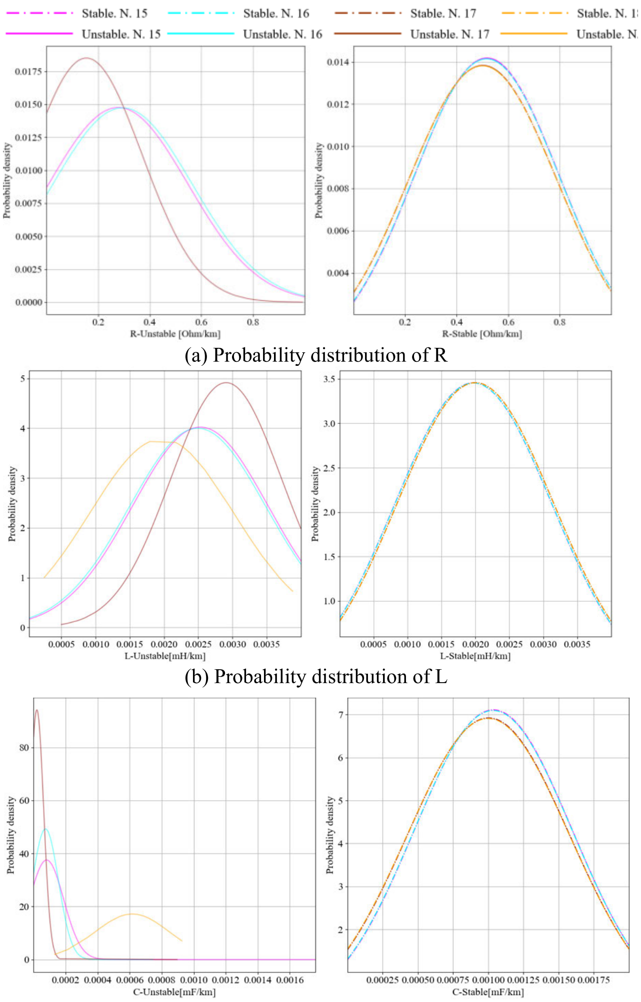

(a) Probability distribution of R

(b) Probability distribution of L

(c) Probability distribution of C

FIGURE 6. Probability distribution of parameters for each eigenvalue.

Fig. 5 shows the points where the real parts of the eigenvalues 15 to 18, derived through MCS-based SSA, settle in the RHP.

Fig. 5 presents R, L, and C in all unstable areas derived through MCS-based SSA. As shown, generally, the likelihood of occurrence increases at lower values of C as the magnitude of eigenvalues settling in the RHP grows. Through Fig. 6, we propose analyzing the probability distribution of R, L, and C in both stable and unstable states to discern the differences in the frequencies of each R, L, and C in unstable systems that may lead to SSO, compared to their frequencies in stable systems.

Fig 6 shows the probability distribution of R, L, and C that leads to the RHP of their respective eigenvalues, demonstrating a clear distinction between stable and unstable systems. In the case of R, L, and C, the probability distributions within a stable system do not significantly vary with the eigenvalues and tend to concentrate around certain values. In contrast, for unstable systems, the probability distributions of R, L, and C vary across different eigenvalues. Specifically, for R, less than 100 instances are leading to the RHP for the 18th eigenvalue, making it challenging to represent this as a PDF. For the other eigenvalues, the likelihood of inducing system instability in lower ranges is higher compared to a stable system. For L, the number of instances leading the 18th eigenvalue into the unstable region is notably small, and the probability of potentially settling other eigenvalues into the RHP is higher compared to a stable system's L. Regarding C, as shown in the scatter plot, there is a higher potential for system instability at lower points compared to an extremely stable system.

In this paper, the distribution of the resonance frequency is also analyzed. The possibility of SSO in PMSG wind turbines, as verified through the results of SSA, depends on the combination of L and C in the transmission line, with the resonance frequency calculated as $f_{resonance} = \frac{1}{2\pi\sqrt{LC}}$. This allows for the identification of the resonance frequency in all unstable system solutions, contributing to the avoidance of SSO.

Fig. 7 displays the distribution of all resonance frequencies $f_{resonance}$ and their probability distribution in unstable systems as R changes, while Table 2 presents the average values of the probability distribution of $f_{resonance}$ in unstable systems caused by each eigenvalue.

TABLE 2. Mean value of L/C ratio distribution.

Number of eigenvalues	Mean value of resonance frequencies [Hz]	
	Unstable	Stable
15	54.27	20.07
16	51.58	20.32
17	123.57	21.64
18	11.70	21.88

Table 2 displays the resonance frequency determined by the combination of L and C, occurring when each eigenvalue settles in the RHP of the complex coordinate system. SSO refers to vibrations occurring at frequencies below the system's nominal frequency (60Hz), with the probability of SSO increasing when the resonance frequency, determined by L and C, is close to or below the nominal system frequency.

However, for the 17th eigenvalue, the average resonance frequency derived from the ratio of L to C, where it settles in the RHP, corresponds to twice the system frequency, indicating that the vibration occurring when the 17th eigenvalue is solely in the RHP is closer to Super Synchronous Oscillations.

The condition for system instability occurs when at least one eigenvalue settles in the RHP. The 15th and 16th eigenvalues predominantly settle in the RHP, potentially inducing SSO, as the average resonance frequencies derived from these eigenvalues are 54.27 and 51.58 [Hz] respectively. This is lower than the nominal system frequency and close to it compared to a stable system, highlighting the need for caution regarding SSO. Based on this information, system planners can devise strategies to avoid SSO and determine stable levels

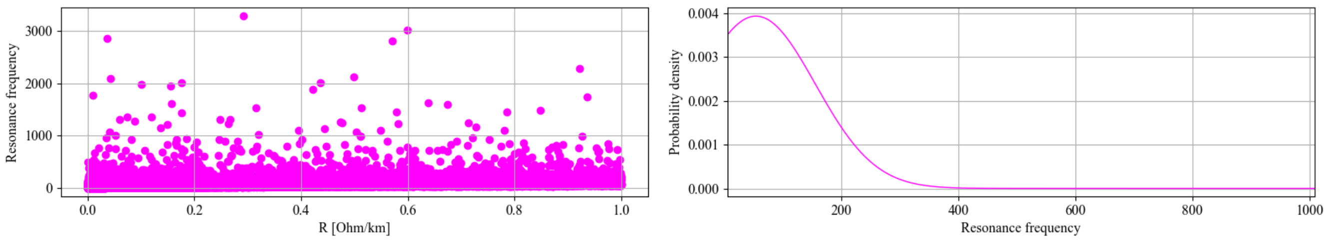

(a) Eigenvalue number 15

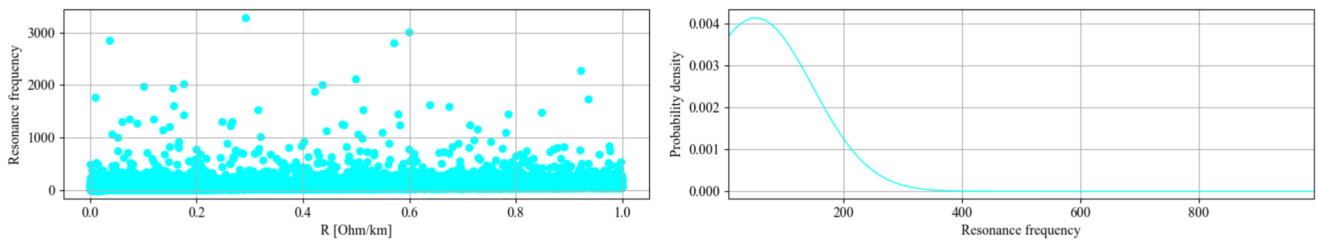

(b) Eigenvalue number 16

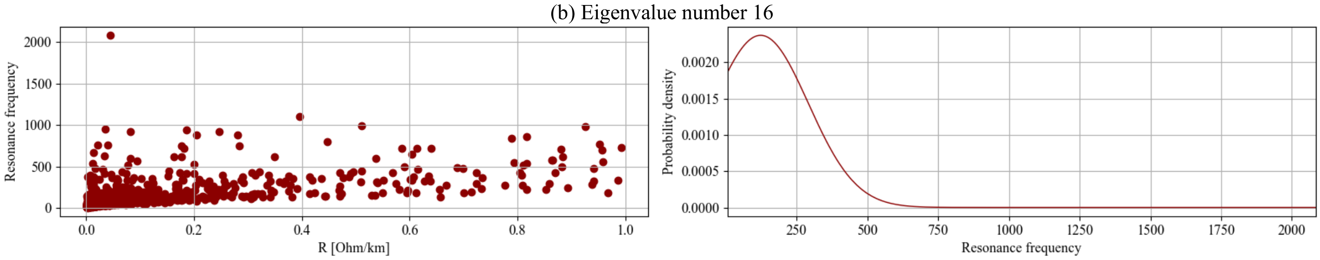

(c) Eigenvalue number 17

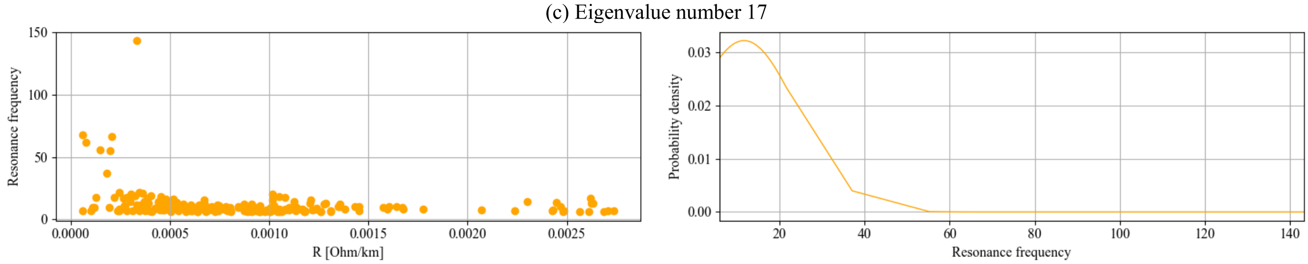

(d) Eigenvalue number 18

FIGURE 7. Probability distribution of resonance frequencies in unstable systems.

of series compensation based on the values of R and L in the transmission line. In essence, Fig. 5 and Fig. 6 provide the potential areas of SSO occurrence for the targeted PMSG wind turbine and offer opportunities to avoid SSO within all unstable systems.

As the number of MCS iterations increases, so does the amount of data for analysis. When integrating actual PMSG wind turbines, the range of specific data will likely be provided. While Fig. 5 and Fig. 6 offer a strong approach for probabilistically analyzing under which conditions of L and C the system may become stable or unstable, this method could potentially lead to excessive time spent on analysis and verification.

Our proposed algorithm, being based on data interpretation, not only broadly demonstrates the system's stable and unstable conditions but also provides applicable values of C for system stability in systems where R and L are definitively given. For example, Fig. 8 shows the distribution of available and unavailable values of C when R is between 0.02∼0.03 [Ω/km] and L is between 0.0017∼0.0018 [mH/km] based on Figs 6 and 7.

As shown in Fig. 8, the squares in blue represent the available values of C, while the stars in green represent the unavailable values of C. Table 3 provides examples of clear solutions by showing sample points from Fig. 8, and Table 4 displays the position and stability of eigenvalues within the complex coordinate system for each sample point.

TABLE 3. Sample points of simulation result.

	Sample point#1	Sample point#2
R [Ω/km]	0.02678	0.02989
L [mH/km]	0.001718	0.001723
C [mF/km]	0.002	0.000684

In Table 4, Sample point#2 is identified as a sub-frequency very close to the system frequency, highly likely to cause resonance. Consistent with previous results, it is recognized

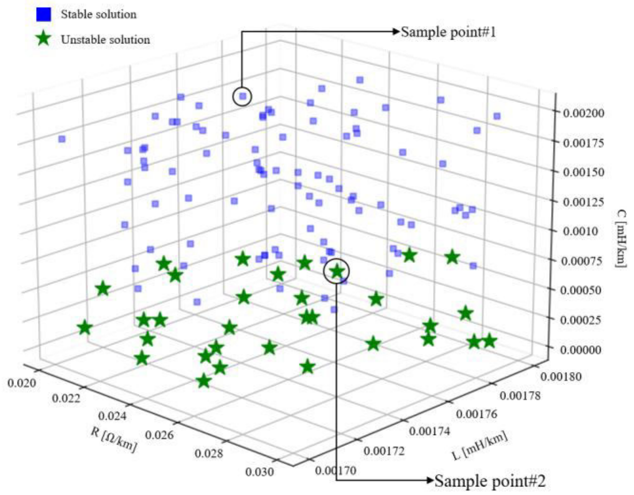

FIGURE 8. Stable solutions of C Based certain range on R and L.

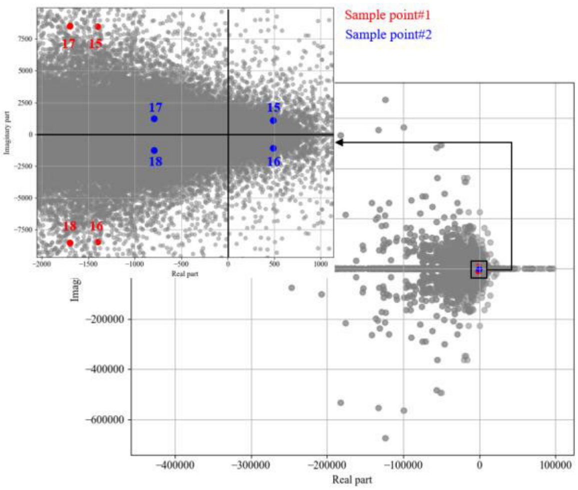

FIGURE 9. Distribution of all eigenvalues according to MCS.

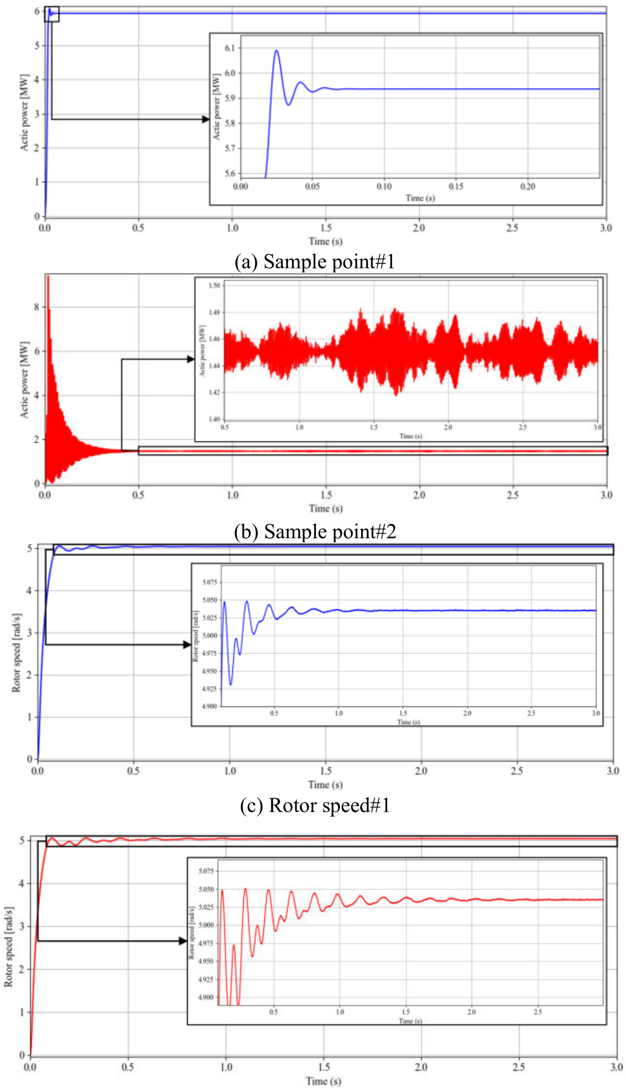

(a) Sample point#1

(b) Sample point#2

(c) Rotor speed#1

(d) Rotor speed#2

FIGURE 10. Active power of PMSG wind turbine at POI for each sample point.

TABLE 4. Stable status of each sample point.

Number of eigenvalues	Position in the complex coordinate system	
	Sample point#1	Sample point#2
15	LHP	RHP
16		
17		LHP
18		
$f_{resonance}$	33.89	57.88
Status	Stable	Unstable

as an unstable system due to eigenvalues 15 and 16 settling in the RHP. During this condition, the output of the PMSG wind turbine can become very unstable, and vibrations may not fully attenuate, necessitating system planners to choose solutions that can avoid SSO.

The solutions proposed in Table 3 and Table 4 allow users to easily make selections and judgments for any range of R and L. Even beyond the range of RLC applied in this paper, applications can be easily adapted with a sufficient number of MCS iterations. Furthermore, while this paper adopts MCS groups to analyze SSO based on the RLC combination of the PMSG wind turbine using the sensitivity matrix, the application of MCS groups enables the analysis of mechanical vibrations according to the design of the PMSG wind turbine and vibration analysis based on control parameters. Moreover, it can be easily applied to the development and control systems of power systems where stability can be analyzed through SSA.

Fig. 9 shows the distribution of all 15 to 18 eigenvalues derived through MCS and marks the points obtained when parameters from each sample point are inputted.

VI. SIMULATION VALIDATION WITH SIMULINK

In this paper, the PMSG wind turbine is modeled through MATLAB/SIMULINK, and it is verified that the results of the algorithm proposed in the paper match the results of the EMTDC model. Fig. 10 shows the graph of the active power at the POI (Point of Interconnection) when applying the sample point from Table 3.

As shown in Fig. 10, for sample point#1, the output of the PMSG wind turbine is stable, whereas for sample point#2, there is significant fluctuation in the active power during a transient period of 0.3 seconds, and continuous output variations occur even within the steady-state region, verifying that the system is unstable.

In this study, the time-domain validation is performed using the active power response at the POI, which is directly related to the system-level stability and oscillatory behavior.

It should be noted that additional internal electrical variables such as reactive power, DC-link voltage, machine speed, and terminal voltage are not included in the present validation, as the primary objective of this work is to identify SSO-prone parameter regions based on eigenvalue analysis and MCS rather than to provide a full EMT-level controller performance assessment.

This limitation will be addressed in future work through more comprehensive EMT-level simulations.

VII. CONCLUSION

In this paper, an MCS-based framework for evaluating the small-signal stability of PMSG wind turbines has been proposed. To reduce computational complexity, a sensitivity matrix-based clustering approach was applied, enabling efficient identification of dominant parameters affecting critical oscillatory modes. The simulation results demonstrated that the effective output of the PMSG wind turbine system, modeled in MATLAB/SIMULINK, exhibits distinct oscillatory behavior under unstable parameter combinations.

The proposed framework provides a systematic approach for identifying stability characteristics of grid-connected PMSG wind turbine systems and can be extended to various control systems utilizing small-signal stability analysis. In particular, the sensitivity information offers practical guidance for controller parameter adjustment by indicating both the direction of influence on eigenvalues and the stability boundaries in the parameter space.

In this study, the analysis primarily focuses on transmission-line parameter variations and their impact on oscillatory stability. Although the effects of control parameters, such as PLL bandwidth, and operating condition variations, such as wind speed, are recognized as important factors influencing system dynamics, they are not explicitly considered in the present framework.

Future work will extend the proposed methodology to incorporate control-related MCS and design-related MCS for a more comprehensive stability assessment of grid-connected PMSG wind turbine systems. In addition, the integration of the proposed framework with HVDC systems will be investigated to evaluate its applicability for efficient long-distance transmission. The impact of wind speed variability on eigenvalue migration will also be investigated in future work.

REFERENCES

[1] H. H. Cho, V. Strezov, and T. J. Evans, "A review on global warming potential, challenges and opportunities of renewable hydrogen production technologies," *Sustain. Mater. Technol.*, vol. 35, Apr. 2023, Art. no. e00567.

[2] A. Moghadasi, A. Sarwat, and J. M. Guerrero, "A comprehensive review of low-voltage-ride-through methods for fixed-speed wind power generators," *Renew. Sustain. Energy Rev.*, vol. 55, pp. 823–839, Mar. 2016.

[3] E. Muljadi, M. Singh, and V. Gevorgian, "Fixed-speed and variable-slip wind turbines providing spinning reserves to the grid," in *Proc. IEEE Power Energy Soc. Gen. Meeting*, Jun. 2013, pp. 1–5.

[4] D. Zhou, F. Blaabjerg, T. Franke, M. Tønnes, and M. Lau, "Comparison of wind power converter reliability with low-speed and medium-speed permanent-magnet synchronous generators," *IEEE Trans. Ind. Electron.*, vol. 62, no. 10, pp. 6575–6584, Oct. 2015.

[5] Z. Maheshwari, K. Kengne, and O. Bhat, "A comprehensive review on wind turbine emulators," *Renew. Sustain. Energy Rev.*, vol. 180, Jul. 2023, Art. no. 113297.

[6] N. Verma, N. Kumar, S. Gupta, H. Malik, and F. P. García Márquez, "Review of sub-synchronous interaction in wind integrated power systems: Classification, challenges, and mitigation techniques," *Protection Control Modern Power Syst.*, vol. 8, no. 1, Dec. 2023.

[7] W. Ren and E. Larsen, "A refined frequency scan approach to sub-synchronous control interaction (SSCI) study of wind farms," *IEEE Trans. Power Syst.*, vol. 31, no. 5, pp. 3904–3912, Sep. 2016.

[8] D. Sun, X. Xie, Y. Liu, K. Wang, and M. Ye, "Investigation of SSTI between practical MMC-based VSC-HVDC and adjacent turbogenerators through modal signal injection test," *IEEE Trans. Power Del.*, vol. 32, no. 6, pp. 2432–2441, Dec. 2017.

[9] L. Wang, X. Xie, Q. Jiang, H. Liu, Y. Li, and H. Liu, "Investigation of SSR in practical DFIG-based wind farms connected to a series-compensated power system," *IEEE Trans. Power Syst.*, vol. 30, no. 5, pp. 2772–2779, Sep. 2015.

[10] D. N. Walker, C. E. J. Bowler, R. L. Jackson, and D. A. Hodges, "Results of subsynchronous resonance test at mohave," *IEEE Trans. Power App. Syst.*, vol. PAS-94, no. 5, pp. 1878–1889, Sep. 1975.

[11] J. Shair, X. Xie, L. Wang, W. Liu, J. He, and H. Liu, "Overview of emerging subsynchronous oscillations in practical wind power systems," *Renew. Sustain. Energy Rev.*, vol. 99, pp. 159–168, Jan. 2019.

[12] R. N. Damas, Y. Son, M. Yoon, S.-Y. Kim, and S. Choi, "Subsynchronous oscillation and advanced analysis: A review," *IEEE Access*, vol. 8, pp. 224020–224032, 2020.

[13] K. Gu, F. Wu, and X.-P. Zhang, "Sub-synchronous interactions in power systems with wind turbines: A review," *IET Renew. Power Gener.*, vol. 13, no. 1, pp. 4–15, Jan. 2019.

[14] V. B. Virulkar and G. V. Gotmare, "Sub-synchronous resonance in series compensated wind farm: A review," *Renew. Sustain. Energy Rev.*, vol. 55, pp. 1010–1029, 2015.

[15] C. Wang, C. Liu, J. Yu, and S. Xu, "Research on sub-synchronous oscillation characteristics between PMSG-based wind farms and weak AC grids based on Prony method," in *Proc. IEEE 3rd Conf. Energy Internet Energy Syst. Integr. (EI2)*, Changsha, China, Nov. 2019, pp. 2781–2786.

[16] Y. Li, X. Yuan, J. Li, H. Xiao, Z. Xu, and Z. Du, "Novel grid-forming control of PMSG-based wind turbine for integrating weak AC grid without sacrificing maximum power point tracking," *IET Gener., Transmiss. Distribution*, vol. 15, no. 10, pp. 1613–1625, May 2021.

[17] G. Li, Y. Chen, A. Luo, and H. Wang, "An enhancing grid stiffness control strategy of STATCOM/BESS for damping sub-synchronous resonance in wind farm connected to weak grid," *IEEE Trans. Ind. Informat.*, vol. 16, no. 9, pp. 5835–5845, Sep. 2020.

[18] W. T. Cochran, J. W. Cooley, D. L. Favin, H. Helms, R. Kaenel, W. Lang, G. C. Maling, D. Nelson, C. M. Rader, and P. D. Welch, "What is the fast Fourier transform?" *Proc. IEEE*, vol. 15, no. 2, pp. 45–55, Oct. 1967.

[19] Y. Xia, B. K. Johnson, Y. Jiang, N. Fischer, and H. Xia, "A new method based on artificial neural network, wavelet transform and short time Fourier transform for subsynchronous resonance detection," *Int. J. Electr. Power Energy Syst.*, vol. 103, pp. 377–383, Dec. 2018.

[20] G. Feng, H. Qifei, H. Zhiguo, and Z. Baohui, "The research of sub synchronous oscillation in PMSG wind farm," in *Proc. IEEE PES Asia–Pacific Power Energy Eng. Conf. (APPEEC)*, Oct. 2016, pp. 1883–1887.

[21] J. Sun, ‘‘Small-signal methods for AC distributed power systems–A review,’’ *IEEE Trans. Power Electron.*, vol. 24, no. 11, pp. 2545–2554, Nov. 2009.
[22] D. Xie, Y. Lu, J. Sun, and C. Gu, ‘‘Small signal stability analysis for different types of PMSGs connected to the grid,’’ *Renew. Energy*, vol. 106, pp. 149–164, Jun. 2017.
[23] S. Zhao, N. Wang, R. Li, B. Gao, B. Shao, and S. Song, ‘‘Sub-synchronous control interaction between direct-drive PMSG-based wind farms and compensated grids,’’ *Int. J. Electr. Power Energy Syst.*, vol. 109, pp. 609–617, Jul. 2019.
[24] H. Liu, X. Xie, J. He, T. Xu, Z. Yu, C. Wang, and C. Zhang, ‘‘Subsynchronous interaction between direct-drive PMSG based wind farms and weak AC networks,’’ *IEEE Trans. Power Syst.*, vol. 32, no. 6, pp. 4708–4720, Nov. 2017.
[25] L. Yuan, K. Meng, J. Huang, and Z. Y. Dong, ‘‘Investigating subsynchronous oscillations caused by interactions between PMSG-based wind farms and weak AC systems,’’ *Int. J. Electr. Power Energy Syst.*, vol. 115, Feb. 2020, Art. no. 105477.
[26] B. Huang, H. Sun, Y. Liu, L. Wang, and Y. Chen, ‘‘Study on subsynchronous oscillation in D-PMSGs-based wind farm integrated to power system,’’ *IET Renew. Power Gener.*, vol. 13, no. 1, pp. 16–26, Jan. 2019.
[27] Q. Shi, G. Wang, L. Fu, L. Yuan, and H. Huang, ‘‘State-space averaging model of wind turbine with PMSG and its virtual inertia control,’’ in *Proc. 39th Annu. Conf. IEEE Ind. Electron. Soc.*, Vienna, Austria, Nov. 2013, pp. 1880–1886.
[28] F. Gao, B. Wu, B. Zhang, Q. He, D. Wang, and W. Ba, ‘‘The mechanism analysis of sub-synchronous oscillation in PMSG wind plants,’’ in *Proc. IEEE Int. Conf. Environ. Electr. Eng. IEEE Ind. Commercial Power Syst. Eur.*, Milan, Italy, Jun. 2017, pp. 1–6.
[29] R. Billinton and R. Karki, ‘‘Application of Monte Carlo simulation to generating system well-being analysis,’’ *IEEE Trans. Power Syst.*, vol. 14, no. 3, pp. 1172–1177, Aug. 1999.
[30] B. D. Rao and K. S. Arun, ‘‘Model based processing of signals: A state space approach,’’ *Proc. IEEE*, vol. 80, no. 2, pp. 283–309, Feb. 1992.
[31] W. Du, W. Dong, and H. F. Wang, ‘‘Small-signal stability limit of a grid-connected PMSG wind farm dominated by the dynamics of PLLs,’’ *IEEE Trans. Power Syst.*, vol. 35, no. 3, pp. 2093–2107, May 2020.

YEONG GEON SON (Member, IEEE) received the B.S. and M.S. degrees from the Department of Electronic and Electrical Engineering, Keimyung University, Daegu, South Korea, in 2020 and 2022, respectively, and the Ph.D. degree from Hanyang University, Seoul, South Korea, in 2025. From 2025 to 2026, he was a Research Assistant with the University of Florida, Gainesville, FL, USA. Since 2026, he has been an Assistant Professor with the Department of Electrical Engineering, Keimyung University. His research interests include integrated energy systems and optimization for power systems.

SUNG-YUL KIM (Member, IEEE) received the B.S. and M.Phil. degrees in electrical engineering from Hanyang University, Seoul, South Korea, in 2007 and 2012, respectively. From 2012 to 2013, he was a Research Assistant with Georgia Institute of Technology, Atlanta, GA, USA. Since 2013, he has been a Professor with the Department of Electrical Engineering, Hanyang University. His main research interests include computer-aided optimization, renewable energy sources for smart grids, and power system reliability.